Milky Way–like Gas Excitation in an Ultrabright Submillimeter Galaxy at $z = 1.6$

N. Sulzenauer[1,2,3,4] , H. Dannerbauer[2,3] , A. Díaz-Sánchez[5] , B. Ziegler[1] , S. Iglesias-Groth[2,3] , and R. Rebolo[2,3,6]

[1] University of Vienna, Department of Astrophysics, Türkenschanzstrasse 17, A-1180 Vienna, Austria; nsulzenauer@mpifr-bonn.mpg.de
[2] Instituto de Astrofísica de Canarias (IAC), E-38205 La Laguna, Tenerife, Spain
[3] Universidad de La Laguna, Dpto. Astrofísica, E-38206 La Laguna, Tenerife, Spain
[4] Max-Planck-Institut für Radioastronomie, Auf dem Hügel 69, 53121 Bonn, Germany
[5] Departamento Física Aplicada, Universidad Politécnica de Cartagena, Campus Muralla del Mar, E-30202 Cartagena, Murcia, Spain
[6] Consejo Superior de Investigaciones Cientficas, E-28006 Madrid, Spain

Abstract

Based on observations with the IRAM 30 m and Yebes 40 m telescopes, we report evidence of the detection of Milky Way–like, low-excitation molecular gas, up to the transition $CO(J = 5\text{–}4)$, in a distant, dusty star-forming galaxy at $z_{CO} = 1.60454$. WISE J122651.0+214958.8 (alias SDSS J1226, the Cosmic Seahorse), is strongly lensed by a foreground galaxy cluster at $z = 0.44$ with a source magnification of $\mu = 9.5 \pm 0.7$. This galaxy was selected by cross-correlating near-to-mid-infrared colors within the full-sky AllWISE survey, originally aiming to discover rare analogs of the archetypical strongly lensed submillimeter galaxy SMM J2135–0102, the Cosmic Eyelash. We derive an apparent (i.e., not corrected for lensing magnification) rest-frame 8–1000 μm infrared luminosity of $\mu L_{IR} = 1.66^{+0.04}_{-0.04} \times 10^{13}\ L_\odot$ and apparent star formation rate $\mu \mathrm{SFR}_{IR} = 2960 \pm 70\ M_\odot\ \mathrm{yr}^{-1}$. SDSS J1226 is ultrabright at $S_{350\mu m} \simeq 170$ mJy and shows similarly bright low-J CO line intensities as SMM J2135–0102, however, with exceptionally small $CO(J = 5\text{–}4)$ intensity. We consider different scenarios to reconcile our observations with typical findings of high-z starbursts, and speculate about the presence of a previously unseen star formation mechanism in cosmic noon submillimeter galaxies. In conclusion, the remarkable low line luminosity ratio $r_{5,2} = 0.11 \pm 0.02$ is best explained by an extended, main-sequence star formation mode—representing a missing link between starbursts to low-luminosity systems during the epoch of peak star formation history.

Unified Astronomy Thesaurus concepts: Galaxy evolution (594); Millimeter astronomy (1061); Starburst galaxies (1570); Infrared galaxies (790); Gravitational lensing (670); CO line emission (262); Star formation (1569); High-redshift galaxies (734); Interstellar medium (847); Molecular gas (1073); Galaxy formation (595); Radio telescopes (1360)

1. Introduction

To get insight into the formation and evolution of massive galaxies at the peak epoch of star formation and black hole activity it is indispensable to study dusty starbursts, so-called submillimeter galaxies (SMGs; see for a review Casey et al. 2014). These dusty star-forming galaxies at a median redshift of $z = 2.3$ (Chapman et al. 2005) are rich in molecular gas (Tacconi et al. 2008), the fuel for star formation. The brightest of these systems are either intrinsically luminous with extreme star formation rates in excess of several hundred to 1000 solar masses per year and/or galaxies that are strongly gravitational lensed by chance alignments with foreground galaxies or galaxy clusters (Negrello et al. 2010). The boosted apparent (sub)millimeter flux of this rare population of low number density $N(S_{500\mu m} > 100\,\mathrm{mJy}) = 0.2\ \mathrm{deg}^{-2}$, and otherwise optically faint or even undetected sources (Dannerbauer et al. 2002), is efficiently identified in wide Herschel or Planck space missions, and South Pole Telescope surveys (see, e.g., Negrello et al. 2010; Vieira et al. 2013; Cañameras et al. 2015).

A remarkable example of a strongly lensed SMG is the serendipitously discovered ultrabright SMM J2135–0102 at $z = 2.326$, the so-called Cosmic Eyelash (Swinbank et al. 2011). Resolved observations of cold gas tracers such as molecular

carbon monoxide (CO) were subsequently utilized in lensed galaxies to test theories of star formation and the conditions of the cold interstellar medium at early cosmic epochs. The assumption that all SMGs are simply scaled-up versions of local universe ultraluminous infrared galaxies (ULIRGs)—mostly gas-rich major mergers (Papadopoulos et al. 2012) that form stars in compact, nuclear disks—is increasingly challenged as high-redshift molecular clouds in star-forming galaxies are observed to inherit their properties from extended, fragmented gas disks, forming massive clumps at a scale of $\lesssim$100 pc (see, e.g., Daddi et al. 2015; Dessauges-Zavadsky et al. 2019). Yet Ivison et al. (2020) reported that the disk of the Cosmic Eyelash is probably smoothly distributed, at least down to ~80 pc scale, reinforcing circumstantial evidence for the heterogeneous population of SMGs, differentiated by their modes of star formation.

In this regard, gravitational lensing promises the detection of low-luminosity systems. Compared to classical SMGs, these systems are forming stars within extended gas disks at an order-of-magnitude lower efficiency (Tacconi et al. 2010). Characterized by low CO excitation profiles (CO SLEDs), as reported by Dannerbauer et al. (2009) in a sample of $z \approx 1.5$ color-selected galaxies (Daddi et al. 2015) and in resolved studies of CO gas in the lensed disk galaxy Cosmic Snake at $z = 1.036$ (Dessauges-Zavadsky et al. 2019), less efficient, slow-mode star formation should be present in low-luminosity, normal galaxies. However, the number of CO detections of these main-sequence galaxies at high redshift is still relatively small (Valentino et al. 2020) and strong evidence for true Milky Way–like cold gas excitation up to high CO transitions

is still lacking or at least inconclusive for this galaxy population.

In this Letter, we present the unusually low, unambiguous Milky Way–like CO excitation profile of SDSS J1226, an ultrabright submillimeter galaxy at $z = 1.60454$, strongly lensed by a galaxy cluster at $z = 0.44$. In Section 2, we present the sample and in Section 3 the observations. Results are shown in Section 4, and we conclude this Letter with the discussion (Section 5). A more complete analysis of the subsample of Herschel-detected, NIR/MIR SMG candidates (including this source) will be presented in N. Sulzenauer et al. (2022, in preparation). In this work we focus on the CO SLED of SDSS J1226. We adopt a flat ΛCDM cosmology using parameters from Planck Collaboration et al. (2016) with $H_0 = 67.8 \pm 0.9$ km s^{-1} Mpc^{-1}, $\Omega_m = 0.308 \pm 0.012$, and $\Omega_\Lambda = 1 - \Omega_m$.

2. Sample Selection

Iglesias-Groth et al. (2017) developed an NIR/MIR color selection technique in order to search for bright SMGs with similar spectral energy distribution (SED) characteristics as the archetypical bright, strongly lensed SMG SMM J2135-0102, the Cosmic Eyelash. MIR sources are cross-matched over the full-sky by correlating the AllWISE[7] catalog from the Wide-field Infrared Survey Explorer (Wright et al. 2010; NIR to MIR colors). Galaxies that verify the NIR/MIR color criterion from Iglesias-Groth et al. (2017):

$$J - K_s > 2.0 \ \wedge \ K_s - W1 > 1.4 \ \wedge$$
$$W1 - W2 > 0.8 \ \wedge \ W2 - W3 < 2.4 \ \wedge \ W3 - W4 > 3.5$$

(in AB magnitudes) are preselected as "Cosmic Eyelash analog" candidates at $z \approx 2$. Subsequent source matching with additional NIR, FIR, and submillimeter data has proven to efficiently select bright SMGs: Díaz-Sánchez et al. (2017) identified the extremely bright SMG WISE J132934.13 +234327.3, the so-called Cosmic Eyebrow, by cross-matching between NIR/MIR selected candidates, Planck[8] full-sky point-source catalog, and JCMT/SCUBA-2[9] data. Spectroscopic follow-up observations with the IRAM 30 m telescope and IRAM NOEMA detected the brightest CO($J = 3$–2) emission ever for SMGs (Dannerbauer et al. 2019). As part of the same sample, the strongly lensed source GAL-CLUS-022058s was followed up with APEX/nFLASH230 spectroscopy confirming extremely bright CO($J = 5$–4) emission (Díaz-Sánchez et al. 2021).

This method was further modified by correlating Herschel/SPIRE[10] sources with NIR/MIR candidates that do not necessarily match all five color criteria, but are in close distance to 28 strong lensing clusters from the Sloan Giant Arcs Survey (Oguri et al. 2012). Due to the availability of archival Hubble Space Telescope (HST) optical data for all of the clusters, the giant arcs were further matched with bright, cospatial AllWISE candidates within $2''$. We have found eight candidates, with $1.5 < z_{\rm phot} < 2.5$; two of them have high apparent infrared luminosities $\mu L_{IR} > 10^{13}$ $L_\odot$ and flux $S_{350\mu m} > 100$ mJy, whereas AllWISE J122651.04+214958.8

is the brightest of the sample with FIR flux $S_{350\mu m} = 170$ mJy. Although it does not fulfill the NIR–color criteria from Iglesias-Groth et al. (2017) nor the one from Díaz-Sánchez et al. (2017), which are based on the Cosmic Eyelash SED, the Herschel FIR flux does agree very well with the behavior of SMG SEDs. This can be explained by large galaxy-to-galaxy variation in the optical–NIR domain due to the combination of dust geometry, star formation history, and extinction (see, e.g., da Cunha et al. 2015). The main discrepancy between the formal NIR/MIR color demarcations and the color indices found for galaxy SDSS J1226 are shallower indices $W1 - W2 \approx 0.3$ instead of > 0.8 and $W3 - W4 \approx 2.2$, whereas $W4$ is only detected as an upper limit implying that the true index might be even more distant from the demarcation index $W3 - W4 > 3.5$. Furthermore, $W2 - W3 \approx -0.2$, although within the criterion definition, is especially low compared to the reported sample values of Iglesias-Groth et al. (2017). Nevertheless, SDSS J1226 is consistently brighter than the Cosmic Eyelash by a factor of $\sim$2 in all WISE bands, but shows lower flux toward FIR wavelengths; see Table 1 for additional photometric catalog data from VizieR at CDS.[11]

On the basis of its position, color, and brightness, we confidently identify the supposed optical counterpart of the Herschel/SPIRE source in sufficiently resolved HST/ACS images.[12] The corresponding giant radial arc is located $\sim 15''$ north to the brightest cluster galaxy (BCG) in the galaxy cluster SDSS J1226+2149 at redshift $z = 0.435 \pm 0.009$ (Bayliss et al. 2011). Therefore, we postulate that the strongly lensed galaxy at coordinates $\alpha = 12^{\rm h}26^{\rm m}51\overset{s}{.}05$ and $\delta = +21°49'58\overset{''}{.}80$ (J2000) is the source of bright NIR–FIR emission. No optical/NIR spectroscopic redshifts of this source are published in the literature. Figure 1 shows the HST/ACS background image at the position of the bright Herschel/SPIRE source. Due to its extraordinary brightness and distinctive morphology, we take the liberty to designate this lensed galaxy as the Cosmic Seahorse.

3. Observations and Data Reduction

3.1. Observations

3.1.1. IRAM 30 m Telescope

We observed the source with the IRAM 30 m telescope heterodyne millimeter receiver EMIR (Carter et al. 2012) by employing the spectroscopic blind line search technique. Starting with the photometric redshift estimate of $z \sim 2$, the CO($J = 2$–1) or CO($J = 3$–2) emission line is expected to lie within the 3 mm atmospheric window, accessible by the EMIR E0 frontend (73–117 GHz). After detecting a strong line at $\approx$88.5 GHz and assuming the redshifted CO($J = 2$–1) transition, we switched the frontend to E1 (125–184 GHz). A second signal was successfully identified in the 2 mm atmospheric window at $\approx$132.8 GHz, the CO($J = 3$–2) line. Based on this improved redshift estimate, CO($J = 5$-4) emission was then observed with E2 (202–274 GHz) at 221.3 GHz. The observations were conducted in position switching mode. We utilized the FTS200 spectrograph as the backend at a frequency resolution of $\sim$200 kHz. The first week of observations (project 086-18, PI: H. Dannerbauer) was regularly scheduled in visitor mode. Between May and November of 2018, the project entered the observing pool. Over 6 days of

---

Table 1
Archival Photometry Associated with Source SDSS J1226-A

Wavelength (μm) (1)	Flux Density[a] (mJy) (2)	AB Mag.[a,b] (mag) (3)	Beam Size (″) (4)	Observatory/Instrument (5)
0.577	0.0007 ± 0.0001	24.3 ± 0.15	~ 0.1	HST/ACS F606W
0.797	0.0022 ± 0.0002	23.0 ± 0.1	~ 0.1	HST/ACS F814W
1.248	0.020 ± 0.002	20.6 ± 0.11	< 1.2	UKIDSS J
1.635	0.034 ± 0.003	20.1 ± 0.1	< 1.2	UKIDSS H
2.201	0.13 ± 0.03	18.6 ± 0.26	< 1.2	UKIDSS K_s
3.4	0.496 ± 0.019[c]	17.2 ± 0.04	6.1	WISE W1
4.6	0.653 ± 0.025[c]	16.9 ± 0.04	6.4	WISE W2
11.6	0.525 ± 0.13[c]	17.1 ± 0.27	6.5	WISE W3
22.1	~ 3.8[c,d]	~ 14.9[d]	12.0	WISE W4
160	87 ± 31	11.5 ± 0.4	11.6	Herschel/PACS
250	172 ± 9	10.8 ± 0.06	18.5	Herschel/SPIRE
350	170 ± 13	10.8 ± 0.08	25.3	Herschel/SPIRE
500	115 ± 12	11.2 ± 0.1	36.9	Herschel/SPIRE

Notes.
[a] Uncorrected for source magnification.
[b] AB magnitudes are calculated using $AB = -2.5 \times \log_{10} S_\nu/[\text{Jy}] + 8.9$, and uncertainties are from a linear approximation.
[c] Flux densities are calculated using the prescription from Wright et al. (2010).
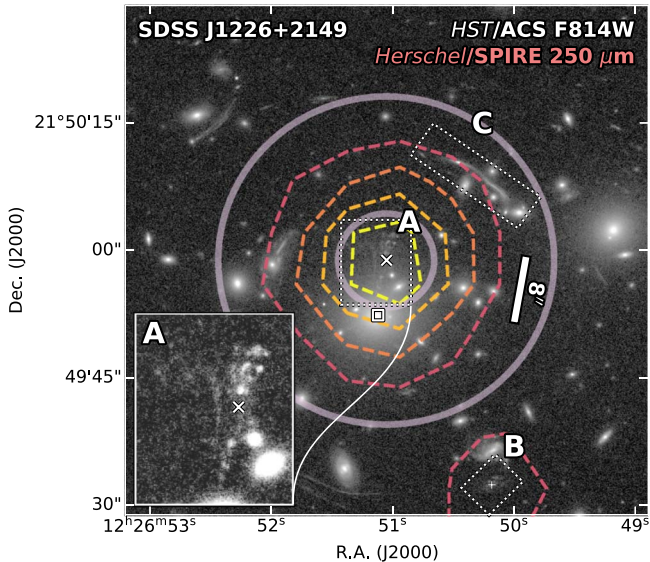[d] Upper limit.

Figure 1. Background image centered on the Herschel/SPIRE flux centroid of source SDSS J1226-A (Cosmic Seahorse) marked by the white cross. HST/ACS F814W data are used to show the presumed optical counterpart (inset with stellar foreground emission gradient masked out) of the FIR-bright source, visible as a strongly lensed radial arc projected north to the BCG (square) of a strongly lensing galaxy cluster at $z = 0.435 \pm 0.009$ (Bayliss et al. 2011; Oguri et al. 2012). Boxes denote main image A, possible counter-image B (white plus), and arc SDSS J1226-C that belongs to a different galaxy at similar redshift, $z = 1.605$, as SDSS J1226-A (Oguri et al. 2012). Herschel/SPIRE 250 μm contour levels at [2, 3, 4, 5]σ confidence intervals above the local background noise level of $\sigma \approx 3.4$ mJy/beam trace the bright FIR source's location. The IRAM 30 m telescope HPBW at 221 GHz ($\approx 11{.}''6$), corresponding to CO($J = 5$–4), is marked by the inner lilac ring, while the outer circle shows the lowest-resolution single-dish HPBW, CO($J = 1$–0) from Yebes 40 m telescope, at $\approx 39{.}''1$, all beam sizes fall in between these two values.

observations, a total of 11.0 hr effective on-source integration time was acquired for the presented multi-J CO line measurements. Overall, weather conditions were acceptable with a median optical depth of $\tau_{255\,\text{GHz}} \approx 0.5$. Notably, however, receiver interference caused baseline ripples in the spectra that needed to be carefully removed.

3.1.2. Yebes 40 m Telescope

Our observations of the redshifted CO($J = 1$–0) line (44.3 GHz) were performed with the new Nanocosmos Q-band receiver, operating between 31.3 and 50.6 GHz (Tercero et al. 2021), installed at the Yebes 40 m telescope (project 20B013, PI: H. Dannerbauer). This frontend consists of two high electron mobility transistor (HEMT) cold amplifiers that cover horizontal and vertical polarization. The signal is obtained using fast Fourier transform spectrometers, covering eight subbands of 2.5 GHz bandwidth and continuous 38 kHz resolution. Over 12 days of observations between 2020 October and November, we collected scans of our source with effective on-source time of 37.2 hr with better than average optical depth of $\tau_{255\,\text{GHz}} = 0.080$. We report the most distant detection of molecular gas at $z = 1.60454$ with the Yebes 40 m telescopes (see, e.g., Tercero et al. 2020).

3.2. Data Reduction

For on-site data reduction, the software GILDAS[13] with package CLASS was used (Pety 2005). To identify spectral lines at the anticipated noise threshold of $T_A^* = 0.25$ mK, the spectra are binned to 500 km s^{-1} and typical observing time per setting were 4 hr in total. Significant line signals are masked for manual baseline removal with a polynomial function of order $n = 3$ within an observed-frame frequency window of $\Delta\nu \approx 1.5$ GHz centered on the signal. After gathering all observations from the pool, individual scans were dropped in order to maximize the signal-to-noise content per spectral bin. For this reason, we developed a simple CLASS script `rmse_selection_function` that is publicly available on GitHub.[14] Up to a specific, nonparametric rms threshold, it filters all scans within the 4 GHz sideband structure of the EMIR FTS200 data by their ranked baseline noise contribution. Adjusting to the background noise level, the frequency channels are rebinned between 13 and 33 km s^{-1} (rest-frame) corresponding to the 99.7% confidence

---

[13] https://www.iram.fr/IRAMFR/GILDAS
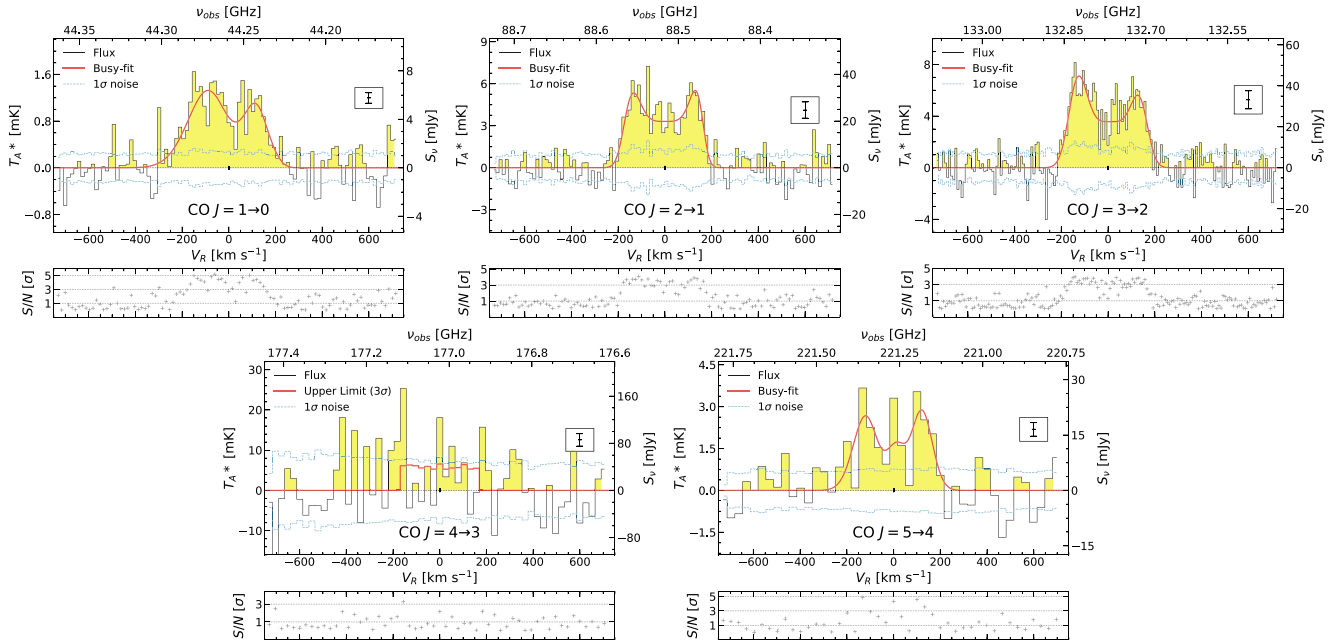[14] https://github.com/NiSZR/rmse_selection_function

Figure 2. CO line spectra of transitions CO($J = 1$–0) from Yebes 40 m radio telescope, and CO($J = 2$–1), CO($J = 3$–2), CO($J = 4$–3), and CO($J = 5$–4) from IRAM 30 m telescope in units of Kelvin and milli-Jansky. Boxed error bars give $\pm 2\sigma$ calibration uncertainties. The lower panels show the S/N values per binned channel in units of background noise rms (blue dashed spectrum). rms noise levels per channel bins are [1.20, 6.2, 7.9, 50.5, 5.3] mJy, respectively. Red curves are flux models fits that are used to calculate the velocity-integrated fluxes. Flux of CO($J = 4$–3) is regarded as a 3σ upper-limit measurement.

level of the line intensity per bin at the position of the spectral line. To convert the corrected main beam brightness temperature to flux density, we fitted a parabola to the values from Velilla Prieto et al. (2017) with sensitivities of approximately 7.56 Jy K^{-1}, 6.31 Jy K^{-1}, and 6.00 Jy K^{-1} in the 1 mm, 2 mm, and 3 mm atmospheric windows. Yebes 40 m telescope 44.3 GHz observations are converted using the factor 4.82 Jy K^{-1}. The total uncertainty of the flux calibration is assumed to be less than 10%. Final data visualization and flux calculation are performed in Python with modules numpy (Harris et al. 2020) and astropy (Astropy Collaboration et al. 2013).

4. Results

4.1. CO SLED

Figure 2 shows the flux densities for the detected CO spectra of SDSS J1226, and Figure 3 gives a comparison between the apparent CO line intensities with error bars at a 3σ confidence level. We were able to blindly identify four bright emission lines with intensity $I_{CO} \equiv \int_{\Delta v} S_{CO} dv > 1.0$ Jy km s^{-1} for corresponding rotational molecular transitions CO($J = 1$–0)[15], CO($J = 2$–1), CO($J = 3$–2), and CO($J = 5$–4). The binned $\Delta V = 500$ km s^{-1} CO features are detected at the level of $S_{CO} = 4.2 - 23$ mJy, corresponding to signal-to-noise ratios (S/Ns) as high as S/N $= 48$ in the case of CO($J = 3$–2). The transition CO($J = 4$–3) is undetected and thus treated as a 3σ upper-limit estimate.[16] We measure a line-averaged redshift of $z_{CO} = 1.604543 \pm 0.00001$.

The CO line profiles match among the transition levels, resembling symmetric double horns with consistent line widths FWHM $= 350 \pm 25$ km s^{-1} (median). This value, however, is

---

[15] This is the most distant line detection with the Yebes 40 m telescope.

[16] Close to the edge of the 2 mm window, foreground noise dominates the line signal as this region is heavily contaminated by the atmospheric H$_2$O feature, leading to a nondetection for CO($J = 4$–3) at 177.014 GHz.
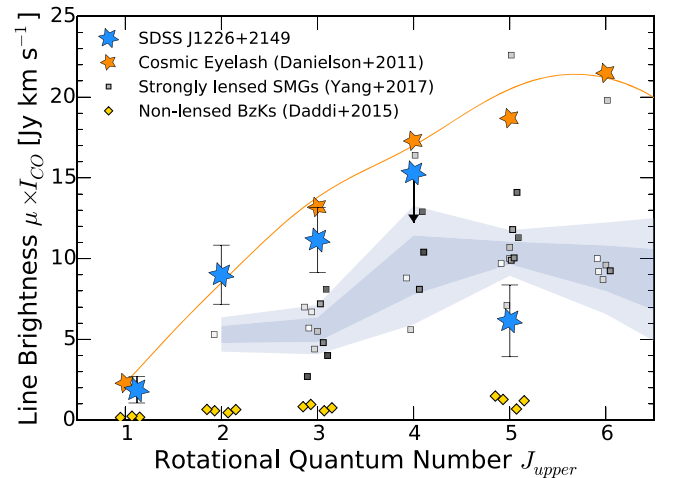

Figure 3. Velocity-integrated line intensity $I_{CO} \equiv \int S_{CO} dv$ comparison of cosmic noon galaxies. IRAM 30 m and Yebes 40 m telescope measurements of SDSS J1226 (blue stars) are compared to the results of SMM J2135–0102 magnified by $\mu = 32$ (orange stars); the orange curve corresponds to the LVG model presented in Danielson et al. (2011). Error bars are shown at a 3σ confidence interval. Velocity-integrated intensity for CO($J = 4$–3) is given as a 3σ upper limit. At $J_{upper} \leqslant 3$, SDSS J1226 is (nearly) as bright as the Cosmic Eyelash and substantially brighter than the Herschel-selected, lensed SMG sample from Yang et al. (2017) (gray squares). Shaded regions indicate the 1σ and 2σ confidence levels of the bootstrapped intensity distribution of the aforementioned SMG sample. Yellow diamonds are Daddi et al. (2015) non-lensed, normal star-forming galaxies.

on the lower end, compatible with the FWHM of the Bothwell et al. (2013) SMG's median at 500 ± 150 km s^{-1} (MAD).

Strikingly, the line intensities for $J_{upper} \leqslant 3$ are comparable to that of the Cosmic Eyelash at a magnification of $\mu = 32$ (lensed by a galaxy cluster at $z = 2.3$; Swinbank et al. 2010; Danielson et al. 2011) while substantially brighter than the strongly lensed Herschel-selected SMGs (in principle, galaxy–galaxy lensing) from the *H*-ATLAS catalog compiled by

Yang et al. (2017). Based exclusively on low-J_{upper} lines, SDSS J1226 is one of the brightest known SMGs on the sky. Only Planck-selected SMGs host consistently brighter interstellar medium (ISM) lines (see, e.g., Harrington et al. 2021).

As a result of high source magnification, SDSS J1226 exhibits *ultrabright* low-J_{upper} CO intensities. However, the trend is reversed for CO($J = 5$–4) where we observe reduced brightness, below the average of the *H*-ATLAS comparison sample. Line luminosity measurements are performed by employing the relationship by Solomon & Vanden Bout (2005),

$$L'_{CO} = 3.25 \times 10^7 \, I_{CO} \, \nu_{obs}^{-2} \, D_L^2 \, (1 + z)^{-3}, \quad (1)$$

in K km s^{-1} pc^2 with ν_{obs} in GHz and D_L in Mpc. To put the intrinsic brightness into context, the line luminosities $L'_{CO(3-2)}$, after correction for magnification, are $(18.2 \pm 1.5)/\frac{\mu}{9.5}$, $(12.1 \pm 0.1)/\frac{\mu}{32}$, $(38 \pm 8)/\frac{\mu}{6}$, and 9.2 ± 2 ($\times 10^9$ K km s^{-1} pc^2) for SDSS J1226, SMM J2135–0102, *H*-ATLAS SMG mean, and BzK normal galaxies' mean. More exceptionally, we obtain $r_{5,2} = L'_{CO(5-4)}/L'_{CO(2-1)} = 0.11 \pm 0.02$, the lowest value yet reported during the first four billion years of cosmic time ($z \geqslant 1.5$; Dannerbauer et al. 2009; Daddi et al. 2015; Valentino et al. 2020), indicating that individual ISM properties do not necessarily follow a common, universal evolution with redshift (see, e.g., Popping et al. 2014; Boogaard et al. 2020) but can depend strongly on galaxy-wide properties such as, e.g., molecular gas fraction. The subthermal excitation of typically bright transitions (Bothwell et al. 2013; Carilli & Walter 2013), as shown in Figure 4, indicates that the molecular medium of SDSS J1226 is less dense and/or hot than typically observed for infrared-luminous, $z \gtrsim 2$ systems (Papadopoulos et al. 2012).

4.2. Additional Properties

4.2.1. Strong Gravitational Lensing Analysis

Since SDSS J1226 is strongly lensed by a galaxy cluster, the physical interpretation of this galaxy is highly dependent on the magnification factor μ. We employed the public software Lenstool[17] (Kneib et al. 1993; Jullo et al. 2007) to derive the lensing model by utilizing the dual pseudo-isothermal elliptical mass distribution (PIEMD; Limousin et al. 2005) for each foreground dark matter halo component. Positions and magnitudes of foreground cluster members were extracted with SExtractor (Bertin & Arnouts 1996) from HST/ACS two-channel maps. We matched visually similar features among the arclets, by color and morphology. In Figure 5, the identified image families are shown. The lensing model predicts a mean magnification of $\mu = 9.5 \pm 0.7$ averaged over the full giant arc SDSS J1226-A. It is successful in predicting the approximate locations, 0″2 rms, of possible counter-images of which three were initially identified (SDSS J1226-A-north, -A-south, and -B). Table 2 provides coordinates and individual magnification factors of the strongly lensed components within the galaxy. For the central halo, an elliptical mass distribution is predicted. Furthermore, the primary deflector parameter values for SDSS J1226+2149 are ellipticity $e = 0.449$, position angle P.A. $= 36°59$, core radius $r_{core} = 27.64$ kpc, cut radius $r_{cut} = 1500$ kpc, and normalization $\sigma_{PIEMD} = 865$ km s^{-1}. The line-of-sight velocity dispersion of the cluster $\sigma_{1D} = 612$ km s^{-1} is derived from 12 cluster members' spectroscopic redshifts
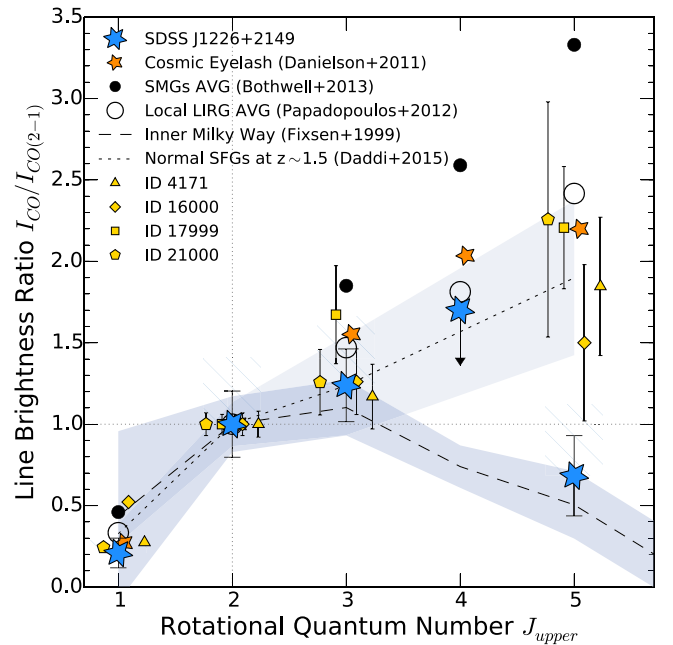

Figure 4. CO excitation profile (CO SLED) of SDSS J1226 (blue stars) normalized to the line intensity of transition CO($J = 2$–1). Error bars indicate 3σ uncertainty confidence intervals. Line excitation of the inner Milky Way (Fixsen et al. 1999; dashed; fills for 95% confidence level) and normal star-forming galaxies at $z \sim 1.5$ (Daddi et al. 2015; yellow symbols; fills same as above) with average values thereof shown as the dotted curve. Median CO excitation for nonlensed SMGs (Bothwell et al. 2013) is indicated by solid circles, and the local LIRG (Papadopoulos et al. 2012) average is shown by open circles. Through transitions CO($J = 1$–0) to CO($J = 3$–2), SDSS J1226 and normal SFGs exhibit similar CO line excitation, although the excitation for transition CO($J = 5$–4) of SDSS J1226 is *significantly lower* than that of normal high-z SFGs, even when considering an underestimation of the CO line width due to erroneous baseline removal (including -1σ shift of baseline level; hatched bars). Intensity for CO($J = 4$–3) is an upper-limit measurement.

provided in Bayliss et al. (2011). In order to estimate the size of the cluster, we calculate the radius $R_{200} = 1.21$ Mpc, which approximates the virial radius, and find the virial mass of the cluster to be $M_{200} = 1.6 \pm 0.8 \times 10^{14}$ $M_\odot$ by employing the relation from Munari et al. (2013). This cluster mass is in concordance with the mass obtained from our lensing model $M_{lens}(< R_{200}) = 2.8 \times 10^{14}$ $M_\odot$. For the fixed redshift of $z = 1.6045$, the critical curves are shown in Figure 5.

4.2.2. Active Galactic Nuclei Diagnostic

As we decided to expand the NIR/MIR color criteria to allow a broader diversity of galaxy properties, the possibility of an AGN contribution needs to be excluded since alternatively it could explain the high observed-frame MIR and FIR emission by processes other than star formation activity. Following the scheme proposed by Secrest et al. (2015) for AllWISE sources, we find observed-frame [3.4]–[4.6] $= 0.3 \pm 0.06$ mag and [4.6]–[12.0] $= -0.2 \pm 0.3$ mag. According to the model tracks relative to the demarcation region of Mateos et al. (2012) these values best match with an aging stellar population at redshift $\sim$1.5, and securely exclude AGN fractions above $f_{AGN} \geqslant 0.2$.

4.2.3. Panchromatic SED Modeling

We used the MAGPHYS[18] code (da Cunha et al. 2008, 2015) to compute synthetic SEDs, from which we

---

[17] https://projets.lam.fr/projects/lenstool/wiki

[18] http://www.iap.fr/magphys/index.html

obtained an apparent rest-frame 8–1000 μm infrared luminosity $\mu L_{\rm IR} = 1.66^{+0.04}_{-0.04} \times 10^{13}$ $L_\odot$. With the apparent infrared luminosity from the best-fitting SED model (reduced $\chi^2 = 0.63$) we computed the star formation rate by assuming a Salpeter initial mass function (IMF) and the conversion factor from Kennicutt (1998). Accordingly, the apparent star formation rate of SDSS J1226 is $\mu{\rm SFR}_{\rm IR} = 2960 \pm 70$ $M_\odot$ yr^{-1}, yielding a magnification corrected star formation rate of ${\rm SFR}_{\rm IR} \approx 300 \times (\mu/9.5)$ $M_\odot$ yr^{-1}. MAGPHYS finds a comparatively lower star formation rate $\mu{\rm SFR} = 737 \pm 17$ $M_\odot$ yr^{-1} (accounting for Chabrier-to-Salpeter IMF conversion of $\Upsilon = 1.8$), stellar mass $\mu M_* = 1.00^{+0.01}_{-0.02} \times 10^{13}$ $M_\odot$, and mass-weighted age age$_{\rm M} = 2.63^{+0.06}_{-0.06}$ Gyr at an average V-band attenuation of $A_V = 3.61^{+0.1}_{-0.02}$ mag. Although the stellar mass appears to be enhanced by a factor of $\sim$10 while the stellar populations are $\times$(2–3) older, the posterior values are in broad agreement with the average properties of ALESS $z \leqslant 2.7$ SMGs on the star-forming main sequence (da Cunha et al. 2015; Schreiber et al. 2015).

5. Discussion

The discovery of this submillimeter ultrabright source demonstrates the capabilities of our selection method (Díaz-Sánchez et al. 2017; Iglesias-Groth et al. 2017; Dannerbauer et al. 2019) to identify the brightest SMGs on the sky. The Cosmic Seahorse (SDSS J1226) is a previously unknown FIR-bright galaxy at spectroscopic redshift $z_{\rm CO} = 1.60454$ that is strongly lensed by a galaxy cluster at $z = 0.44$ with magnification factor $\mu = 9.5 \pm 0.7$. The galaxy's image is split up into three magnified images—A-south, A-north with a total extent of $\theta_{\rm arc} \approx 8''2$, and image B. Since counter-image B is less affected by shear, it might, in future studies, serve as a standard to constrain a potential flux bias caused by differential magnification.

Strong lensing directly affects the obtained IRAM 30 m and Yebes 40 m telescope measurements of the CO lines that are much brighter, without magnification correction, than typically observed for Herschel-selected SMGs but comparable in brightness to the CO line flux of the Cosmic Eyelash. However, the CO($J = 5$–4) flux and thus warmer/dense gas contribution is significantly below that of the Cosmic Eyelash (Danielson et al. 2011) and even below the $J_{\rm upper} = 5$ excitation of normal star-forming galaxies at similar redshift (Daddi et al. 2015). To relax our assumption on the shape of the CO SLED, line intensities in Figure 4 are normalized to $I_{\rm CO(2-1)}$ that also trace more diffuse, cirrus-like, and cool gas. Hence, the normalized brightness at high $J_{\rm upper}$ is used as a proxy diagnostic for the dense and/or warm gas involved in star formation (Weiss et al. 2007). Typically, 870 μm-selected SMGs (see, e.g., Bothwell et al. 2013) show SLEDs with a broad excitation plateau at $J_{\rm upper} \approx 5 - 7$. Similar CO SLEDs are also observed for main-sequence star-forming galaxies (Daddi et al. 2015; Valentino et al. 2020), although at a lower median excitation. Noted by Popping et al. (2014), the line ratio CO($J = 5$–4) over CO($J = 2$–1) does scale particularly strong with star formation activity and molecular gas surface density at all redshifts. Thus, a low line luminosity ratio $r_{5,2}$ is commonly interpreted as to broadly trace cold gas conditions (see, e.g., Valentino et al. 2020) that are ultimately governed by energy and momentum injection from star formation activity, consequently driving the CO excitation.

Accordingly, CO SLEDs of distant galaxies such as SMGs or normal star-forming galaxies are found to be well explained by a two-component model of the ISM, a cool and warm phase, with intensity contributions depending on the physical properties of the cool gas (Bothwell et al. 2013; Daddi et al. 2015). Purely Milky Way–like CO excitation, with very little contribution from dense and warm gas, has never been reported in an early universe or cosmic noon galaxy before. Although some high-redshift normal SFGs show significantly similar $J_{\rm upper} \leqslant 3$ excitation (Dannerbauer et al. 2009; Daddi et al. 2015). Even in consideration of high amounts of low surface brightness gas— that might lead to an underestimation of line width and thus could cause issues with background subtraction—the CO excitation of $J_{\rm upper} = 5$ in SDSS J1226 is by $\sim$3σ confidence level below the median of normal SFGs (Daddi et al. 2015). At face value, a CO SLED with $r_{5,2} = 0.11 \pm 0.02$ predominantly resembles single-component excitation that might originate from physical conditions possibly not dissimilar to those observed in the 4 kpc molecular region of the inner Milky Way (see Figure 4; Fixsen et al. 1999). We acknowledge the existence of comparably low $r_{5,2}$ ratios in at least one of the Valentino et al. (2020) reported nonlensed main-sequence galaxies, i.e., $r_{5,2} \approx 0.13$ in ID 35349 at $z = 1.25$. But since none of these sources fulfill both criteria of having (1) a sufficient number of high-fidelity, low-J CO flux measurements to confirm *true* Milky Way–like CO SLEDs at a high significance level and (2) can be strictly defined as bona fide cosmic noon galaxies at $1.5 < z < 3$, we claim that these sources do not challenge our interpretation of the Cosmic Seahorse.

To explain the unusual CO SLED, we consider three possible scenarios. First, measurement errors originating from either calibration, pointing, and/or line width underestimation might be responsible for the low $J_{\rm upper} = 5$ excitation. However, only an unfortunate combination of these observational effects together could produce the magnitude of the effect in the data.

Second, a short-lived phenomenon—like a tidal bridge, commonly seen in LIRGs—might indeed produce similarly low excitation mainly due to a local decrease of the high-density gas fraction (Zhu et al. 2003; Weiss et al. 2007). Together with a possible magnification bias, this spatially confined component might then be preferentially amplified. We deem this scenario as less likely, since our lensing map does not predict strong differential magnification beyond $\gtrsim$10%.

Third, a previously unseen mechanism of early universe star formation, acting on high-mass, low-$L_{\rm IR}$ systems, might be present. The last scenario is the most attractive, as the number counts of SMGs are intrinsically steep (see, e.g., Negrello et al. 2010) and although ultra- and hyper-luminous infrared systems (HyLIRGs) dominate star formation activity beyond $z \gtrsim 1$ (Le Floc'h et al. 2005) still a large fraction of cosmic star formation rate density occurs in $L_{\rm IR} \lesssim 10^{12}$ $L_\odot$ systems (Rodighiero et al. 2011). But also from a theoretical perspective, low excitation of an ISM with star formation surface density $\Sigma_{\rm SFR} = 0.46 \pm 0.02$ $M_\odot$ yr^{-1} kpc^{-2} (based on the magnified area of the main arc) is predicted by the model[19] of Narayanan & Krumholz (2014) to match well with our CO SLED observations at reduced $\chi^2_r = 1.21$. The predicted line ratio is $r_{5,2}(\Sigma_{\rm SFR}) = 0.25 \pm 0.01$ compared to observational $r_{5,2} = 0.11 \pm 0.02$. Following this line of evidence, we conclude that the Cosmic Seahorse

---

[19] https://sites.google.com/a/ucsc.edu/krumholz/codes/co-sled

might most likely intrinsically belong to an underexplored population of dusty, low L_{IR} systems with high gas masses—in disguise of classical ULIRGs—that form stars in extended, clumpy disks at low efficiency. We have no strong argument to support a major merger scenario, like broad line widths, but can also not refute it. Additional measurements at high-J CO transitions, resolved interferometry of the continuum, and better constraints on the source magnification are indispensable to further eliminate one of the proposed hypotheses.

Given the remarkable low $r_{5,2}$ line ratio, and disregarding magnification bias, we postulate that the Cosmic Seahorse (SDSS J1226) hosts Milky Way–like cold gas conditions—similar to those seen in the inner Galactic region—but in the distant universe. Contrary to the more typical high-excitation regime of cold gas in SMGs, this novel source with overall star-forming main-sequence characteristics shows unique interstellar medium properties for a strongly lensed, ultrabright galaxy at $S_{500\mu m} > 100$ mJy. Providing further circumstantial evidence to this hypothesis, we find that the locus of intrinsic stellar mass over star formation rate, including all discussed uncertainties (see Section 4.2), falls within $^{+1}_{-2} \times \sigma$ of that of main-sequence galaxies (Schreiber et al. 2015) at the same cosmic epoch.

Moreover, in virtue of its bright CO emission lines, SDSS J1226 could also serve as a new reference source for extended, low-efficiency star formation at high redshift. Follow-up observations should be able to spatially resolve the main giant arc—in analogy to resolved studies of SMM J2135–0102 (Swinbank et al. 2011; Ivison et al. 2020)—into individual giant molecular clouds, further enabling insight into a massive galaxy at a truly complementary track to local ULIRG-like galaxy evolution. At decl. $\delta \simeq +22°$, both ALMA and IRAM NOEMA interferometers would be capable of expanding line observations beyond CO($J = 5$–4) at high spatial resolution to ultimately verify the unusual CO excitation profile among the Cosmic Seahorse's molecular clouds. The discovery of low gas excitation in an otherwise typical dusty star-forming galaxy emphasizes the inferred diversity of yet unexplored pathways in early galaxy assembly.

Appendix
Lensing Map

Figure 5 shows the lensing model constraints and corresponding Table 2 lists the co-ordinates with magnification factors of the identified image families.

Table 2
List of Constraints for the Lensing Model by Matching Image Families among the Arclets

ID[a] (1)	R.A. (°) (2)	Decl. (°) (3)	μ[b] (4)
1.A-north	186.71274	21.83322	8.1 ± 1.1
1.A-south	186.71290	21.83244	4.4 ± 0.8
1.B	186.70915	21.82564	2.2 ± 0.3
2.A-north	186.71267	21.83357	7.3 ± 0.7
2.A-south	186.71302	21.83212	1.9 ± 0.4
2.B	186.70902	21.82578	2.3 ± 0.3
3.A-north	186.71244	21.83355	6.0 ± 0.6
3.A-south	186.71296	21.83210	1.7 ± 0.4
3.B	186.70919	21.82579	2.3 ± 0.3
4.A-north	186.71251	21.83381	7.2 ± 0.6
4.A-south	186.71306	21.83192	1.2 ± 0.3
4.B	186.70894	21.82592	2.3 ± 0.3
1.C-east	186.71021	21.83615	12 ± 3
1.C-west	186.70894	21.83530	17 ± 5

Notes. Coordinates are for epoch J2000.
[a] All entries start formally with"SDSS J1226-". The digit refers to the ID of the family of images coming from the same region within the source galaxy. The letter and positional argument indicates the ID of the image seen in the image plane.
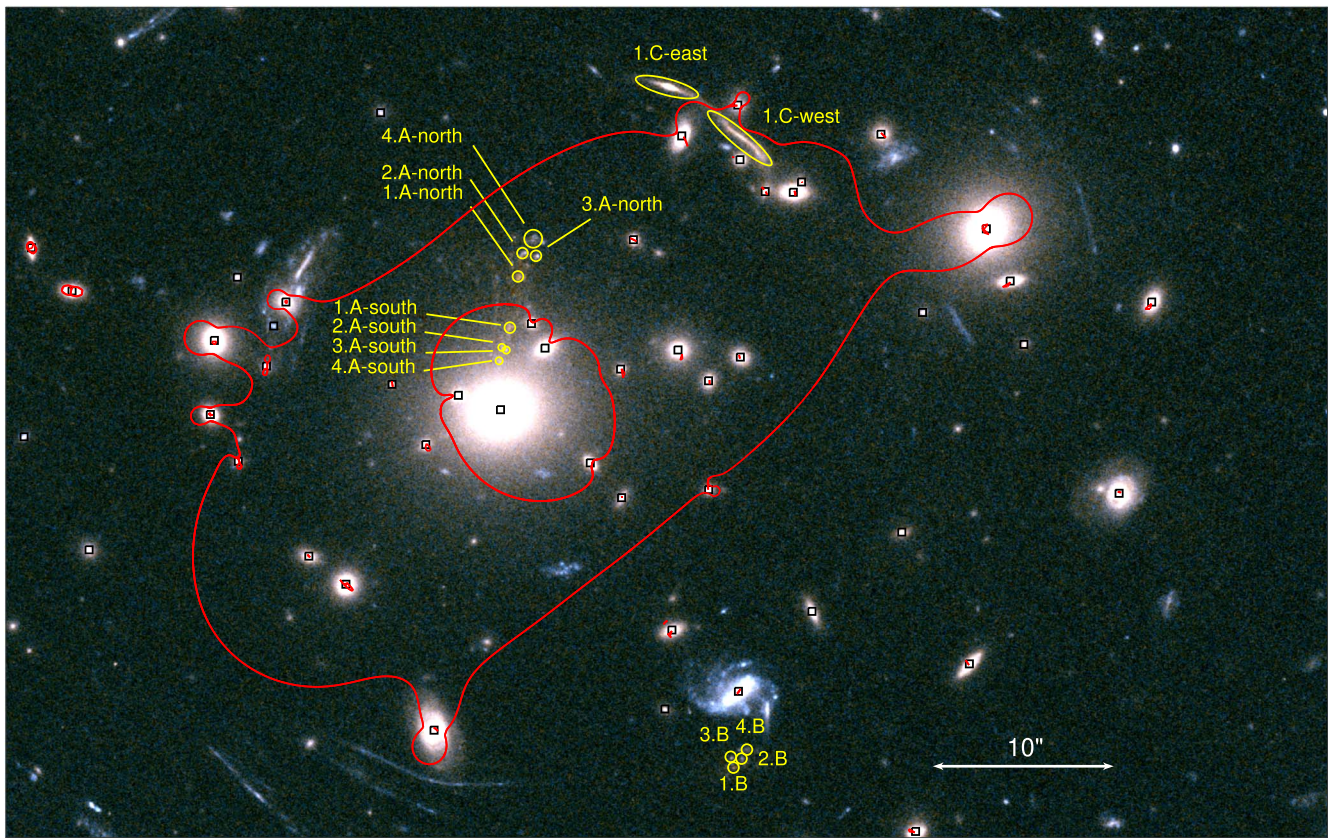[b] Magnification factor.

Figure 5. Two-channel HST/ACS map showing filter bands F555W (cyan) and F814W (orange) with overplotted lensing analysis constraints. Foreground galaxy cluster members at $z \approx 0.435$ are indicated as black squares. The rest-frame UV-bright clumps that are used to model the gravitational lensing effect in the three images of the galaxy SDSS J1226 (A-north, A-south, and B) are marked in yellow and there are four families (1, 2, 3, and 4). Galaxy SDSS J1226-C is the same redshift as our target, yet a distinct system, and also lensed into two images, C-east and C-west. Shown in red are the modeled critical curves of the foreground galaxy cluster potential, for the same redshift as the Cosmic Seahorse and source SDSS J1226-C.

ORCID iDs

N. Sulzenauer https://orcid.org/0000-0002-3187-1648
H. Dannerbauer https://orcid.org/0000-0001-7147-3575
A. Díaz-Sánchez https://orcid.org/0000-0003-0748-4768
B. Ziegler https://orcid.org/0000-0003-2856-1080
S. Iglesias-Groth https://orcid.org/0000-0003-0618-0615
R. Rebolo https://orcid.org/0000-0003-3767-7085

References

Astropy Collaboration, Robitaille, T. P., Tollerud, E. J., et al. 2013, A&A, 558, A33
Bayliss, M. B., Hennawi, J. F., Gladders, M. D., et al. 2011, ApJS, 193, 8
Bertin, E., & Arnouts, S. 1996, A&AS, 117, 393
Boogaard, L. A., van der Werf, P., Weiss, A., et al. 2020, ApJ, 902, 109
Bothwell, M. S., Smail, I., Chapman, S. C., et al. 2013, MNRAS, 429, 3047
Cañameras, R., Nesvadba, N. P. H., Guery, D., et al. 2015, A&A, 581, A105
Carilli, C. L., & Walter, F. 2013, ARA&A, 51, 105
Chapman, S. C., Blain, A. W., Smail, I., et al. 2005, ApJ, 622, 772
Carter, M., Lazareff, B., Maier, D., et al. 2012, A&A, 538, A89
Casey, C. M., Narayanan, D., & Cooray, A. 2014, PhR, 541, 45
da Cunha, E., Charlot, S., & Elbaz, D. 2008, MNRAS, 388, 1595
da Cunha, E., Walter, F., Smail, I. R., et al. 2015, ApJ, 806, 110
Daddi, E., Dannerbauer, H., Liu, D., et al. 2015, A&A, 577, A46
Danielson, A. L. R., Swinbank, A. M., Smail, I., et al. 2011, MNRAS, 410, 1687
Dannerbauer, H., Lehnert, M. D., Lutz, D., et al. 2002, ApJ, 573, 473
Dannerbauer, H., Daddi, E., Riechers, D. A., et al. 2009, ApJL, 698, L178
Dannerbauer, H., Harrington, K., Díaz-Sánchez, A., et al. 2019, AJ, 158, 34

Dessauges-Zavadsky, M., Richard, J., Combes, F., et al. 2019, NatAs, 3, 1115
Díaz-Sánchez, A., Iglesias-Groth, S., Rebolo, R., et al. 2017, ApJL, 843, L22
Díaz-Sánchez, A., Dannerbauer, H., Sulzenauer, N., Iglesias-Groth, S., & Rebolo, R. 2021, ApJ, 919, 48
Fixsen, D. J., Bennett, C. L., & Mather, J. C. 1999, ApJ, 526, 207
Harrington, K. C., Weiss, A., Yun, M. S., et al. 2021, ApJ, 908, 95
Harris, C. R., Millman, K. J., van der Walt, S. J., et al. 2020, Natur, 585, 357
Iglesias-Groth, S., Díaz-Sánchez, A., Rebolo, R., et al. 2017, MNRAS, 467, 330
Ivison, R. J., Richard, J., Biggs, A. D., et al. 2020, MNRAS, 495, L1
Jullo, E., Kneib, J.-P., Limousin, M., et al. 2007, NJPh, 9, 447
Kennicutt, R. C. 1998, ApJ, 498, 541
Kneib, J.-P., Mellier, Y., Fort, B., et al. 1993, A&A, 273, 367
Le Floc'h, E., Papovich, C., Dole, H., et al. 2005, ApJ, 632, 169
Limousin, M., Kneib, J.-P., & Natarajan, P. 2005, MNRAS, 356, 309
Mateos, S., Alonso-Herrero, A., Carrera, F. J., et al. 2012, MNRAS, 426, 3271
Munari, E., Biviano, A., Borgani, S., et al. 2013, MNRAS, 430, 2638
Narayanan, D., & Krumholz, M. R. 2014, MNRAS, 442, 1411
Negrello, M., Hopwood, R., De Zotti, G., et al. 2010, Sci, 330, 800
Oguri, M., Bayliss, M. B., Dahle, H., et al. 2012, MNRAS, 420, 3213
Papadopoulos, P. P., van der Werf, P. P., Xilouris, E. M., et al. 2012, MNRAS, 426, 2601
Pety, J. 2005, in SF2A-2005: Semaine de l'Astrophysique Francaise, ed. F. Casoli et al. (Paris: EdP-Sci), 721
Planck Collaboration, Ade, P. A. R., Aghanim, N., et al. 2016, A&A, 594, A13
Popping, G., Pérez-Beaupuits, J. P., Spaans, M., et al. 2014, MNRAS, 444, 1301
Rodighiero, G., Daddi, E., Baronchelli, I., et al. 2011, ApJL, 739, L40
Schreiber, C., Pannella, M., Elbaz, D., et al. 2015, A&A, 575, A74
Secrest, N. J., Dudik, R. P., Dorland, B. N., et al. 2015, ApJS, 221, 12
Solomon, P. M., & Vanden Bout, P. A. 2005, ARA&A, 43, 677
Swinbank, A. M., Smail, I., Longmore, S., et al. 2010, Natur, 464, 733

Swinbank, A. M., Papadopoulos, P. P., Cox, P., et al. 2011, ApJ, 742, 11
Tacconi, L. J., Genzel, R., Smail, I., et al. 2008, ApJ, 680, 246
Tacconi, L. J., Genzel, R., Neri, R., et al. 2010, Natur, 463, 781
Tercero, B., Cernicharo, J., Cuadrado, S., et al. 2020, A&A, 636, L7
Tercero, F., López-Pérez, J. A., Gallego, J. D., et al. 2021, A&A, 645, A37
Valentino, F., Daddi, E., Puglisi, A., et al. 2020, A&A, 641, A155
Vieira, J. D., Marrone, D. P., Chapman, S. C., et al. 2013, Natur, 495, 344
Velilla Prieto, L., Sánchez Contreras, C., Cernicharo, J., et al. 2017, A&A, 597, A25
Weiss, A., Downes, D., Neri, R., et al. 2007, A&A, 467, 955
Wright, E. L., Eisenhardt, P. R. M., Mainzer, A. K., et al. 2010, AJ, 140, 1868
Yang, C., Omont, A., Beelen, A., et al. 2017, A&A, 608, A144
Zhu, M., Seaquist, E. R., & Kuno, N. 2003, ApJ, 588, 243